An improved, time-efficient approach to extract accurate distance restraints for NMR^2 structure calculation.

Aditya Pokharna[a], Felix Torres[a], Harindranath Kadavath[a], Julien Orts*[b], and Roland Riek*[a]

[a]Laboratory of Physical Chemistry, ETH, Swiss Federal Institute of Technology, HCI F217, Vladimir-Prelog-Weg 2, 8093 Zürich, Switzerland

[b]University of Vienna, Faculty of Life Sciences, Department of Pharmaceutical Sciences, Althanstrasse 14, 2F 353, A-1090, Vienna, Austria

*Correspondence to : Roland Riek (roland.riek@phys.chem.ethz.ch) and Julien Orts (julien.orts@univie.ac.at)

Abstract

Exact Nuclear Overhauser Enhancement (eNOE) yields highly accurate, ensemble averaged ^{1}H-^{1}H distance restraints with an accuracy of up to 0.1 $Å$ for the multi-state structure determination of proteins as well as for Nuclear Magnetic Resonance Molecular Replacement (NMR^2) to determine the structure of the protein-ligand interaction site in a time-efficient manner. However, in the latter application, the acquired eNOEs lack the obtainable precision of 0.1 $Å$ because of the asymmetrical nature of the filtered NOESY experiment used in NMR^2. This error is further propagated to the eNOE equations used to fit for and extract the distance restraints.

In this work, a new analysis method is proposed to obtain inter-molecular distance restraints from the filtered NOESY spectrum more accurately and intuitively by dividing the NOE cross-peak by the corresponding diagonal peak of the ligand. The method termed diagonal-normalized eNOEs was tested on the data acquired by Torres et al. (Torres et al., 2020) on the complex of PIN1 and a small, weak-binding phenylimidazole fragment. NMR^2 calculations performed using the distances derived from diagonal-normalised eNOEs yielded the right orientation of the fragment in the binding pocket, and produced a structure that more closely resembles the benchmark X-ray structure (2XP6) (Potter et al., 2010) with an average heavy atom RMSD of 1.681 $Å$ with respect to it, when compared to the one produced with traditional NMR^2 with an average heavy atom RMSD of 3.628 $Å$. This is attributed to the higher precision of the evaluated distance restraints.

1 INTRODUCTION

Nuclear Magnetic Resonance Molecular Replacement (*NMR*[2]) is a hybrid approach to determine the structure of protein-ligand complexes, utilising a previously determined structure (for example, a X-ray structure or a structure from a protein homolog) of the target protein and combining it with the spatial information extracted by solution state NMR to identify the binding pocket of the protein and the orientation of the ligand inside it (Wälti and Orts, 2018). The major strength of the method is that one does not need to carry out protein resonance assignment to obtain the complex structure. Using *NMR*[2], Orts et al. has been able to solve the structure of various complexes (Torres et al., 2020); (Wälti and Orts, 2018); (Orts et al., 2016) accurately (up to 1 Å) within a few days of measurement and analysis. The *NMR*[2] structure calculation workflow is detailed in (Orts and Riek, 2020) and relies on acquiring precise inter-molecular distance restraints.

In *NMR*[2], the ^{13}C, ^{15}N-labelled protein and non-labelled ligand are mixed and measured together using the F1-[^{15}N,^{13}C]-filtered [^{1}H,^{1}H]-NOESY experiment (Zwahlen et al., 1997) to extract the inter-molecular NOE rates and the corresponding distances. This analysis is performed in an in-built module within CYANA structure calculation software (Güntert and Buchner, 2015) called ENORA (Strotz et al., 2017). ENORA fits the NOE buildup curves obtained at multiple mixing times to extract exact cross-relaxation rates (eNOEs) which produces semi-accurate distance restraints with both upper and lower limit (Vögeli et al., 2009).

However, the precision of these inter-molecular distance restraints is much lower (~20% higher tolerance needed) (Strotz et al., 2015) than the bi-directional intra-molecular eNOEs, usually measured inside the protein, from a series of ^{15}N, ^{13}C-resolved [^{1}H,^{1}H]-NOESY experiments that have a precision of 0.1 Å. The lower precision is attributed to the imbalanced magnetisation pathway within the F1-^{15}N, ^{13}C-filtered [^{1}H,^{1}H]-NOESY experiment, the lack of a clean steady state magnetisation at the beginning of the experiment, the unknown spin diffusion contribution (Kalk and Berendsen, 1976) and the complexity involved in extracting distances within ENORA, which further propagates errors arising from the NOESY spectrum.

In this work, we present an alternative approach for extracting cross-relaxation rates from the filtered 2D NOESY spectra that forgoes the need for the sophisticated and time-intensive eNORA calculations and produces more accurate distances. The complex used in this study is that of cis/trans isomerase PIN1 with a low molecular weight fragment, 2-(3-Chlorophenyl)-5-methyl-1H-imidazole-4-carboxylic acid, drawn in Figure A1, whose structure of the interaction site was solved by Torres et. al (Torres et al., 2020), in order to test the *NMR*[2] method for weak binding small molecules. This fragment called Compound 2 in the paper by Torres et al. (Torres et al., 2020) produces very few inter-molecular eNOEs to PIN1, due to its small size (comprising only a few protons) and low binding affinity (760 μM). This makes the de-novo determination of the right pose of the ligand in the binding pocket using *NMR*[2] very challenging.

As we shall see, our approach has been successful in producing better restraints for the PIN1-Compound 2 complex than the standard procedure thereby predicting the right orientation of the ligand in the binding pocket when compared with the X-ray structure of this complex (2XP6) (Potter et al., 2010), which serves as a benchmark to ascertain the accuracy of the *NMR*[2] structures.

2 THEORY

Following the standard NMR theory of the NOESY experiment (Keepers and James, 1984), the proposed analysis arises out of simple approximations made on the fundamental equations used to calculate eNOEs. Every spin pair that produces a cross-peak can be assumed to form a two-spin system. The cross-relaxation rate for a two-spin system (i and j) can be analytically given as (Macura et al., 1986); (Boelens et al., 1988); (Vögeli, 2014):

$$\frac{I_{ij}(t)}{I_{ii}(0)} = \frac{I_{ji}(t)}{I_{jj}(0)} = \frac{-\sigma_{ij}}{\lambda_+ - \lambda_-}(\exp\{-\lambda_- t\} - \exp\{-\lambda_+ t\}) \tag{1}$$

where $I_{ii}(t)$ and $I_{ij}(t)$ represent the peak intensity of the diagonal and the cross-peak in the NOESY spectrum respectively. The cross-relaxation rate, σ_{ij}, further depends on $\lambda_{\pm}$ which are a function of auto-relaxation rates of the two spins, ρ_i and ρ_j.

$$\lambda_{\pm} = \frac{\rho_i + \rho_j}{2} \pm \sqrt{\left(\frac{\rho_i - \rho_j}{2}\right)^2 + \sigma_{ij}^2} \tag{2}$$

The diagonal intensities can be approximated by a single-exponential decay, completely independent of the auto- and cross-relaxation rates of the other spin:

$$I_{ii}(t) = I_{ii}(0) \exp\{-\rho_i t\} \tag{3}$$

Furthermore, under the assumption that $\rho_i \approx \rho_j = \rho$, which holds true for small- to medium-sized proteins, the exponential terms in Equation 1 can be expanded to the second-order as follows:

$$\exp\{-\lambda_{\pm}t\} = \exp\{-(\rho \pm \sigma)t\} = 1 - (\rho \pm \sigma)t + \frac{(\rho \pm \sigma)^2 t^2}{4} \ldots \tag{4}$$

Combining Equations 1, 3 and 4, the following expression can be obtained:

$$\boxed{\frac{I_{ij}(t)}{I_{ii}(t)} = -\sigma_{ij}t} \tag{5}$$

This straightforward expression relates the cross-peak and diagonal intensities at mixing time, t, to the cross-relaxation rate. These quantities can be directly extracted from NOESY spectra recorded at multiple mixing times and fitted with a simple linear model to compute the cross-relaxation rate. This forgoes the need for invoking the ENORA module to fit the NOE build-ups. More importantly, it produces more accurate rates as it only involves directly fitting the experimentally-derived peak build-up intensities once. With the standard approach used in ENORA, the diagonal intensities are fitted in accordance with Equation 3 to extrapolate the auto-relaxation rate, ρ_i and the initial magnetisation, $I_{ii}(0)$. The error introduced to these quantities by imprecise fitting of Equation 3 and low SNR of diagonal peaks is propagated to Equations 1 and 2, which are used to determine σ_{ij}. Furthermore, the imbalance inherent to the F1-[^{15}N,^{13}C]-filtered [^{1}H,^{1}H]-NOESY experiment and the missing ρ_i contributes to the relative error. This error is also compounded in the eNORA approach as the peak intensity data is transformed and used in multiple fitting equations.

The rates determined with the new method proposed here using Equation 5 are termed diagonal-normalised NOEs. The conversion from the obtained cross-relaxation rates to distances can be made via the equations reported in the previous NMR^2 publications (Wälti and Orts, 2018). Please note that in the case of PIN1-Compound 2 complex, the effective correlation time used to convert rates to distances was derived from steric distances found in the fragment (Torres et al., 2020).

However, there is a level of uncertainty still attached to the distance restraints extracted via this method because of the assumption, $\rho_i = \rho_j$, especially for large ligand-protein complexes with weak binding affinities, as ρ_j might be an order of magnitude above ρ_i. A simple test was performed to quantify the uncertainty introduced by the above assumption to the extracted distances. It involved taking artificial distances (3 Å and 5 Å) between spin pairs followed by back calculating the value of the respective cross-relaxation rates. The obtained rates were fed to Equations 1 and 2 with varying assumptions of the values of the auto-relaxation rates (ρ_j and ρ_i). The ratios of magnetisation transfer $\frac{I_{ij}(t)}{I_{ii}(t)}$ were obtained at identical mixing times [40, 60, 90 and 120 ms], as used by Torres et al. (Torres et al., 2020) and fitted according to the Equation 5 in an attempt to reproduce the artificial distances.

The results of the test are detailed in Figure A2 in the Appendix. At the ratio of $\frac{\rho_j}{\rho_i}$=10, the highest measured ratio, generally expected for the complex of a large protein and a small ligand, our method was

able to reproduce the inter-molecular distance with an accuracy of 12.45% for both 3 $Å$ and 5 $Å$. Hence, we propose a distance accuracy of $\pm \sim$10% for our approach. This distance accuracy lies between distances derived from bi-directional eNOEs (0%) and uni-directional eNOEs (20%) (Strotz et al., 2015). It is noted that the software CYANA uses a harmonic potential for a its target function (TF) to accommodate the distance restraints, and as such 0% means that only harmonic potential is involved, whereas 20% distance tolerance indicates the presence of a flat potential from 0%-20% distance followed by the harmonic potential beyond it (Güntert and Buchner, 2015).

3 RESULTS AND DISCUSSION

In order to evaluate the accuracy of the distance extraction method of diagonal-normalised NOEs the PIN1-Compound 2 complex introduced above is used. All the NMR experiments on the PIN1-Compound 2 complex were conducted and the subsequent resonance assignments were performed by Torres et al (Torres et al., 2020) (co-authors in this study). They resolved the structure of the binding pocket using NMR^2 on the inter-molecular, uni-directional, eNOE-derived distance restraints which have an expected accuracy of 20% (Strotz et al., 2015). In this work, we have used their data, recorded on ^{15}N,^{13}C-filtered [^{1}H,^{1}H]-NOESY spectra, to evaluate the performance of the diagonal-normalised eNOE analysis as compared to the the standard eNOE approach (Vögeli et al., 2009); (Vögeli, 2014).
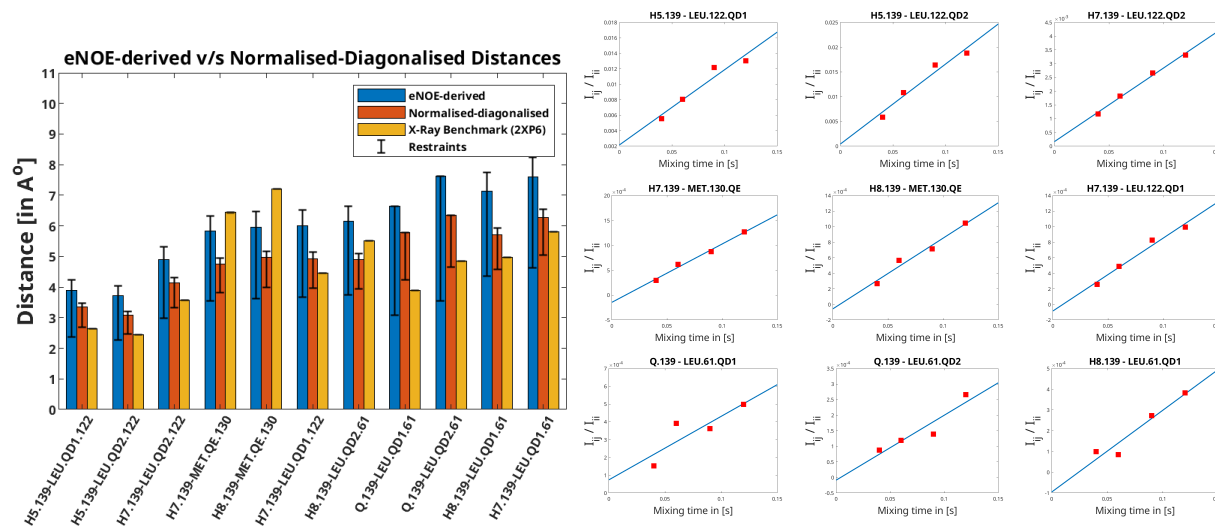
Figure 1: (Left) Distances extracted from F1-[^{15}N,^{13}C]-filtered [^{1}H,^{1}H]-NOESY using the eNOE (blue) and diagonal-normalised approach (red) compared to the benchmark X-ray structure. The bars denote the distances that arise from the cross-relaxation rates from the complex of PIN1 with Compound 2, as given in (Torres et al., 2020). The bars in yellow represent the distances back-calculated from the X-ray structure (2XP6) (Potter et al., 2010). The error bars denote the upper and lower limit restraints produced in CYANA (Güntert and Buchner, 2015) for the extracted distances. A tolerance of 20% and 10% was taken and for the eNOE and the diagonal-normalised approach extracted distances respectively. (Right) The ratio of NOE buildups to the corresponding diagonal peak intensities plotted against mixing time for the PIN1-Compound 2 complex for the diagonal-normalised approach. The data points were fitted using a linear least square fitting model in MATLAB (MATLAB, 2018). The slope denotes the cross-relaxation rate of the given peak, as per Equation 5.

Apart from being more time-efficient and intuitive, this method should also provide more accurate distances, as discussed in the Theory section. The NOE build ups plots, fit linearly according to Equation 5, are depicted in Figure 1 (right). The linear fits mostly tend to zero when mixing time is zero and the

experimental data fits well even at longer mixing times for all cross-peaks. This indicates a lack of significant spin diffusion contribution. Moreover, it is easier to detect spin diffusion with this method compared to the standard approach using eNORA, as it manifests itself as non-linearity in the fitted data. This difference is illustrated in Figure A3 in the Appendix.

The derived distance restraints are also plotted against the conventional eNOE-derived distance restraint and the distances back-calculated from the benchmark X-ray structure (2XP6) (Potter et al., 2010) in Figure 1 (left) (The protons were added to the X-ray structure in CYANA (Güntert and Buchner, 2015)). Indeed, the diagonal-normalised distance restraints better resemble the ones from the X-ray structure (mean difference in the distances being 1.04 ± 0.65 Å) than the ones from the standard approach (mean difference in the distances being 1.57 ± 0.73 Å). The only exceptions being the distances that include the protons from the solvent-exposed Methionine 130.

The inter-molecular distances obtained from the PIN1-Compound 2 complex through the conventional eNORA-based method and the diagonal-normalised approach are plotted in Figure 1. The plots illustrate that the restraints obtained via the latter are tighter by 0.4-1.2 Å. The source of this difference, as discussed in the Theory section, arises from the inherent complexity involved in extracting distances from a filtered 2D-NOESY spectrum.

To evaluate the 10% error estimate deduced in the Theory section further and to study the impact of the diagonal-normalised distance restraints on NMR^2 structure determination, NMR^2 structures of the complex PIN1-Compound 2 were calculated with varying degree of precision of the diagonal-normalised distance restraints (i.e. 0%, 5%, 10%, and 20%) (Table 1). The restraints were input in the NMR^2 algorithm and the output structures were compared to the structure determined in (Torres et al., 2020) using standard eNOEs.

The NMR^2 program screens all potential combinations of methyl groups in protein and protons on the ligand and calculates the complex structure for all of the possibilities without needing protein assignment. The success of an NMR^2 run lies in it being able to discriminate between all the possible structures and pinpoint the right pose of ligand in the binding pocket. This is especially difficult for small fragments like Compound 2, with only 5 distinct protons/methyl groups.

Table 1: Table detailing the results of NMR^2 calculations with distance restraints extracted from eNOE and diagonal-normalised method with varying values of errUni in CYANA.

Method Used	Precision (in % of the given distance)[1]	Does the structure converge up to TF = 2 Å²? (Yes/No)[2]	Target Function of 4 lowest energy conformers (in Å²)	Total number of degenerate lowest energy conformers[3]	RMSD w.r.t to the benchmark (2XP6) (in Å²)
eNORA-based	20%	Yes	[0, 0, 0, 0]	10+	3.63
Diagonal-Normalised	20%	Yes	[0, 0, 0, 0]	5	2.17
Diagonal-Normalised	10%	Yes	[0.03,0.12,0.20,0.73]	1	1.68
Diagonal-Normalised	$\leq$ 5%	No	–	–	–

[1] A precision of x% dictates the value of upper limit and lower limit distance restraints with the upper limit distance restraint being (1+ x%)*(extracted distance) and the lower limit distance restraint being (1- x%)*(extracted distance).

[2] A target function (TF) of less than 2 Å² within NMR^2 is considered a successful structure determination (Orts and Riek, 2020).

[3] The total number of degenerate lowest energy conformers is the number of distinct orientations of the ligand within the binding pocket that were obtained with a CYANA target function (TF) of 0 Å² from NMR^2 calculations.
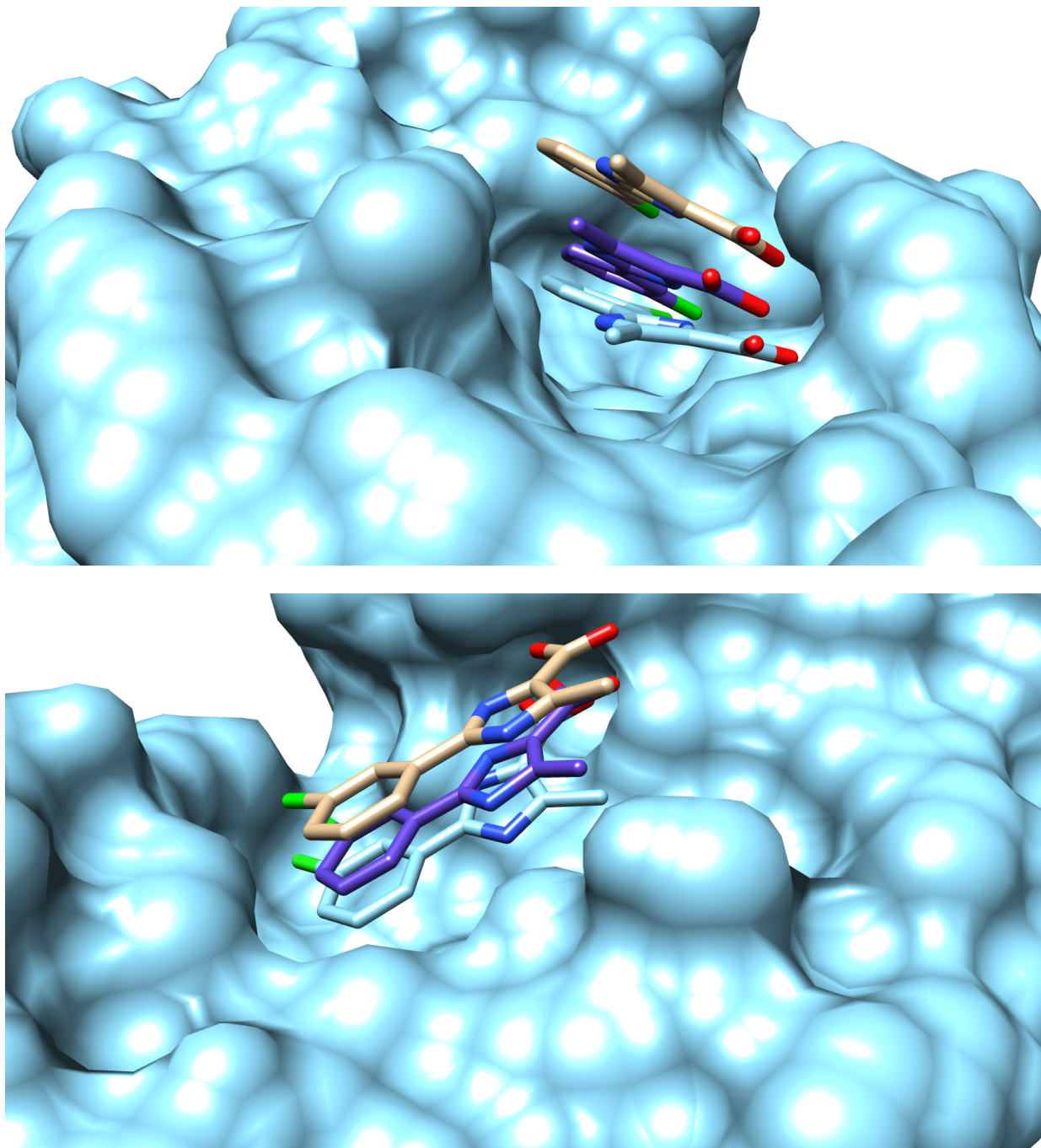
Figure 2: Surface representation of the binding pocket of PIN1 with Compound 2 from two different perspectives. Coloured in cyan is the surface representation of the protein alongside a stick representation of ligand determined by X-ray crystallography studies (2XP6) (Potter et al., 2010). Coloured in brown is the stick representation of the structure of the ligand inside the binding pocket determined by Torres et al. (Torres et al., 2020) with a distance precision of 20% using the standard ENORA approach. Coloured in purple is the structure determined by NMR^2 calculations using the distances extracted via the diagonal-normalised approach with a precision of 10% (refer to Row 3 in Table 1). The nitrogen, oxygen and chlorine atoms on the ligand are coloured blue, red and green respectively.

Table 1 outlines the details of the structure calculation test. The restraints obtained through the eNORA-based method were not good enough and gave rise to more than 10 degenerate structures with a Target

Function (TF) of 0 $Å^2$, meaning that all experimental distance restraints were fulfilled without inconsistency/error in any of the 10 degenerate structures. The structure in which the ligand has the same orientation inside the binding pocket, as the benchmark X-ray structure (2XP6) (Potter et al., 2010), has an RMSD of 3.63 $Å$ with respect to the X-ray structure (2XP6) . Using the diagonal-normalised distance determination procedure with a precision of 20%, a better performance is observed with only 5 degenerate structures with a TF of 0 $Å^2$, which included the complex structure with Compound 2 in the right pose (RMSD of 2.17$Å$). For the anticipated precision of the distance restraints of 10%, the calculation produced only one structure with a TF = 0.03 $Å^2$, coloured in purple in Figure 2, which shows the same orientation as the crystal structure with an RMSD of 1.68 $Å$. This structure superimposes well with the benchmark structure, coloured in cyan in Figure 2. A visual inspection of the binding pocket illustrated in Figure 2 shows that the ligand appears deeper in the binding pocket and better aligned with the crystal structure compared to the structure obtained by traditional, eNORA-based NMR^2. For a distance precision of 5% and below, the calculations did not converge to structures that fulfil the experimental restraints and produce structures below the hard limit of TF < 20 $Å^2$. This is expected since the distance restraints are not of the quality of bidirectional restraints due to the assumption $\rho_i=\rho_j$, the lack of spin diffusion correction and other restrictions inherent to the NMR^2 protocol, such as the use of a previously determined protein structure and combining X-ray and NMR data.

The strength of this approach lies in distinguishing the correct pose of a weak-binding, low molecular weight ligands which gives very few inter-molecular NOEs inside the binding pocket of a larger proteins. Nevertheless, this approach was also tested on the protein-ligand complex of HDM2, a human oncogenic protein, with caylin-1, which presents abundant inter-molecular NOEs. The traditional eNORA-based NMR^2 was successful in characterising the structure of protein-ligand interaction site (7QDQ), as shown in the work of Mertens et al. (Mertens et al., 2022). With the diagonal-normalised approach at 10% precision, we obtained the same pose of caylin-1 in the HDM2 binding site, as Mertens et al., with a TF of 1.52 $Å^2$ and RMSD between the two structures being 0.81 $Å$ (refer to Figure A4 in the Appendix). Furthermore, the calculations made with 15% and 20% precision also matched the predictions of traditional NMR^2 in identifying the right structure. This is further evidence that our approach can at least match the predictions of traditional NMR^2 in the case of strong binders and possibly exceed them in the case of weak binders with less NOEs. It is noted that the presence of multiple configurations/conformations of the ligand in the binding pocket will require detailed eNOE-based multi-state structure calculations (Vögeli et al., 2013); (Ashkinadze et al., 2022).

To sum up, this work proposes an intuitive and time-efficient, alternative method to extract precise distance restraints from a series of filtered-NOESY spectra, that gives, in the system studied, an accurate NMR^2 structure of the protein-ligand interaction site.

4 MATERIALS AND METHOD

No new material was prepared for the sake of this work. The protocol to express and purify the protein and the ligand and to mix them afterwards is detailed in (Torres et al., 2020).

No new NMR experiments were conducted for this work either. The peak intensities from the spectra acquired by Torres et al. were extracted via ccpNMR (Skinner et al., 2016). The intensities were later fit to acquire the rates in the MATLAB Software suite (MATLAB, 2018). The structure calculation were performed by NMR^2 program through CYANA (Güntert and Buchner, 2015). All the structures were displayed and overlaid over each other using the Chimera molecular visualisation tool (Pettersen et al., 2004).

5 ACKNOWLEDGEMENT

We would like to thank the Swiss National Foundation for financial support through the grant number 310030_192646.

183 ## 6 CONFLICT OF INTEREST

184 No conflict of interest.

185 ## 7 DATA AVAILABILITY

186 All relevant data can be obtained upon request.

187 ## BIBLIOGRAPHY

188 Ashkinadze, D., Kadavath, H., Riek, R., and Güntert, P.: Optimization and validation of multi-state
189 NMR protein structures using structural correlations, Journal of Biomolecular NMR, 76, 39–47, doi:
190 10.1007/s10858-022-00392-2, URL https://doi.org/10.1007/s10858-022-00392-2, 2022.

191 Boelens, R., Koning, T. M. G., and Kaptein, R.: Determination of biomolecular structures from proton-
192 proton NOE's using a relaxation matrix approach, Journal of Molecular Structure, 173, 299–311, doi:
193 10.1016/0022-2860(88)80062-0, URL https://www.sciencedirect.com/science/article/pii/0022286088800620,
194 1988.

195 Güntert, P. and Buchner, L.: Combined automated NOE assignment and structure calculation with CYANA,
196 Journal of Biomolecular NMR, 62, 453–471, doi:10.1007/s10858-015-9924-9, URL https://doi.org/10.1007/
197 s10858-015-9924-9, 2015.

198 Kalk, A. and Berendsen, H. J. C.: Proton magnetic relaxation and spin diffusion in proteins, Journal of
199 Magnetic Resonance (1969), 24, 343–366, doi:10.1016/0022-2364(76)90115-3, URL https://www.sciencedirect.
200 com/science/article/pii/0022236476901153, 1976.

201 Keepers, J. W. and James, T. L.: A theoretical study of distance determinations from NMR. Two-
202 dimensional nuclear overhauser effect spectra, Journal of Magnetic Resonance (1969), 57, 404–426, doi:
203 10.1016/0022-2364(84)90257-9, URL https://www.sciencedirect.com/science/article/pii/0022236484902579,
204 1984.

205 Macura, S., Farmer, B. T., and Brown, L. R.: An improved method for the determination of cross-relaxation
206 rates from NOE data, Journal of Magnetic Resonance (1969), 70, 493–499, doi:10.1016/0022-2364(86)90143-5,
207 URL https://www.sciencedirect.com/science/article/pii/0022236486901435, 1986.

208 MATLAB: 9.7.0.1190202 (R2018b), The MathWorks Inc., Natick, Massachusetts, 2018.

209 Mertens, V., Abi Saad, M. J., Coudevylle, N., Wälti, M. A., Finke, A., Marsh, M., and Orts, J.: Elucidation of a
210 nutlin-derivative—HDM2 complex structure at the interaction site by NMR molecular replacement: A
211 straightforward derivation, Journal of Magnetic Resonance Open, 10-11, 100 032, doi:10.1016/j.jmro.2022.
212 100032, URL https://www.sciencedirect.com/science/article/pii/S2666441022000024, 2022.

213 Orts, J. and Riek, R.: Protein—ligand structure determination with the NMR molecular replacement
214 tool, NMR2, Journal of Biomolecular NMR, 74, 633–642, doi:10.1007/s10858-020-00324-y, URL https:
215 //doi.org/10.1007/s10858-020-00324-y, 2020.

216 Orts, J., Wälti, M. A., Marsh, M., Vera, L., Gossert, A. D., Güntert, P., and Riek, R.: NMR-Based Determination
217 of the 3D Structure of the Ligand–Protein Interaction Site without Protein Resonance Assignment, Journal
218 of the American Chemical Society, 138, 4393–4400, doi:10.1021/jacs.5b12391, URL https://doi.org/10.1021/
219 jacs.5b12391, publisher: American Chemical Society, 2016.

220 Pettersen, E. F., Goddard, T. D., Huang, C. C., Couch, G. S., Greenblatt, D. M., Meng, E. C., and Ferrin, T. E.:
221 UCSF Chimera—A visualization system for exploratory research and analysis, Journal of Computational
222 Chemistry, 25, 1605–1612, doi:10.1002/jcc.20084, URL https://onlinelibrary.wiley.com/doi/abs/10.1002/jcc.
223 20084, _eprint: https://onlinelibrary.wiley.com/doi/pdf/10.1002/jcc.20084, 2004.

224 Potter, A., Oldfield, V., Nunns, C., Fromont, C., Ray, S., Northfield, C. J., Bryant, C. J., Scrace, S. F., Robinson,
225 D., Matossova, N., Baker, L., Dokurno, P., Surgenor, A. E., Davis, B., Richardson, C. M., Murray, J. B.,
226 and Moore, J. D.: Discovery of cell-active phenyl-imidazole Pin1 inhibitors by structure-guided fragment
227 evolution, Bioorganic & Medicinal Chemistry Letters, 20, 6483–6488, doi:10.1016/j.bmcl.2010.09.063, URL
228 https://www.sciencedirect.com/science/article/pii/S0960894X10013648, 2010.

229 Skinner, S. P., Fogh, R. H., Boucher, W., Ragan, T. J., Mureddu, L. G., and Vuister, G. W.: CcpNmr
230 AnalysisAssign: a flexible platform for integrated NMR analysis, Journal of Biomolecular NMR, 66,
231 111–124, doi:10.1007/s10858-016-0060-y, URL https://doi.org/10.1007/s10858-016-0060-y, 2016.

232 Strotz, D., Orts, J., Minges, M., and Vögeli, B.: The experimental accuracy of the uni-directional exact NOE,
233 Journal of Magnetic Resonance, 259, 32–46, doi:10.1016/j.jmr.2015.07.007, URL https://www.sciencedirect.
234 com/science/article/pii/S1090780715001597, 2015.

235 Strotz, D., Orts, J., Chi, C. N., Riek, R., and Vögeli, B.: eNORA2 Exact NOE Analysis Program, Journal of
236 Chemical Theory and Computation, 13, 4336–4346, doi:10.1021/acs.jctc.7b00436, URL https://doi.org/10.
237 1021/acs.jctc.7b00436, publisher: American Chemical Society, 2017.

238 Torres, F., Ghosh, D., Strotz, D., Chi, C. N., Davis, B., and Orts, J.: Protein–fragment complex structures
239 derived by NMR molecular replacement, RSC Medicinal Chemistry, 11, 591–596, doi:10.1039/D0MD00068J,
240 URL https://pubs.rsc.org/en/content/articlelanding/2020/md/d0md00068j, publisher: RSC, 2020.

241 Vögeli, B.: The nuclear Overhauser effect from a quantitative perspective, Progress in Nuclear Magnetic
242 Resonance Spectroscopy, 78, 1–46, doi:10.1016/j.pnmrs.2013.11.001, URL https://www.sciencedirect.com/
243 science/article/pii/S0079656513001003, 2014.

244 Vögeli, B., Segawa, T. F., Leitz, D., Sobol, A., Choutko, A., Trzesniak, D., van Gunsteren, W., and Riek,
245 R.: Exact Distances and Internal Dynamics of Perdeuterated Ubiquitin from NOE Buildups, Journal of
246 the American Chemical Society, 131, 17 215–17 225, doi:10.1021/ja905366h, URL https://doi.org/10.1021/
247 ja905366h, publisher: American Chemical Society, 2009.

248 Vögeli, B., Orts, J., Strotz, D., Güntert, P., and Riek, R.: Discrete Three-dimensional Representation of
249 Macromolecular Motion from eNOE-based Ensemble Calculation, CHIMIA, 66, 787–787, doi:10.2533/
250 chimia.2012.787, URL https://chimia.ch/chimia/article/view/2012_787, number: 10, 2012.

251 Vögeli, B., Güntert, P., and Riek, R.: Multiple-state ensemble structure determination from eNOE spectroscopy,
252 Molecular Physics, 111, 437–454, doi:10.1080/00268976.2012.728257, URL https://doi.org/10.1080/00268976.
253 2012.728257, publisher: Taylor & Francis _eprint: https://doi.org/10.1080/00268976.2012.728257, 2013.

254 Wälti, M. A. and Orts, J.: The NMR2 Method to Determine Rapidly the Structure of the Binding
255 Pocket of a Protein–Ligand Complex with High Accuracy, Magnetochemistry, 4, 12, doi:10.3390/
256 magnetochemistry4010012, URL https://www.mdpi.com/2312-7481/4/1/12, number: 1 Publisher: Multi-
257 disciplinary Digital Publishing Institute, 2018.

258 Zwahlen, C., Legault, P., Vincent, S. J. F., Greenblatt, J., Konrat, R., and Kay, L. E.: Methods for Measurement of
259 Intermolecular NOEs by Multinuclear NMR Spectroscopy: Application to a Bacteriophage N-Peptide/boxB
260 RNA Complex, Journal of the American Chemical Society, 119, 6711–6721, doi:10.1021/ja970224q, URL
261 https://doi.org/10.1021/ja970224q, publisher: American Chemical Society, 1997.

2-(3-Chlorophenyl)-5-methyl-1H-imidazole-4-carboxylic acid

Molecular Formula	$C_{11}H_9ClN_2O_2$
Average mass	236.654 Da
Monoisotopic mass	236.035248 Da
ChemSpider ID	25056681
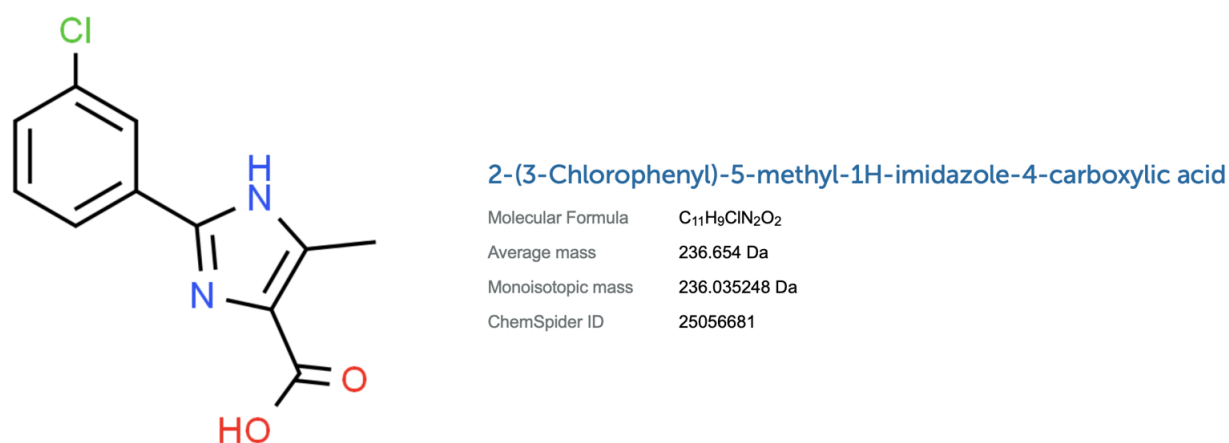
Figure A1: A line representation of Compound 2 (2-(3-Chlorophenyl)-5-methyl-1H-imidazole-4-carboxylic acid) from (Torres et al., 2020). The figure was obtained from ChemSpider (ID:25056681).
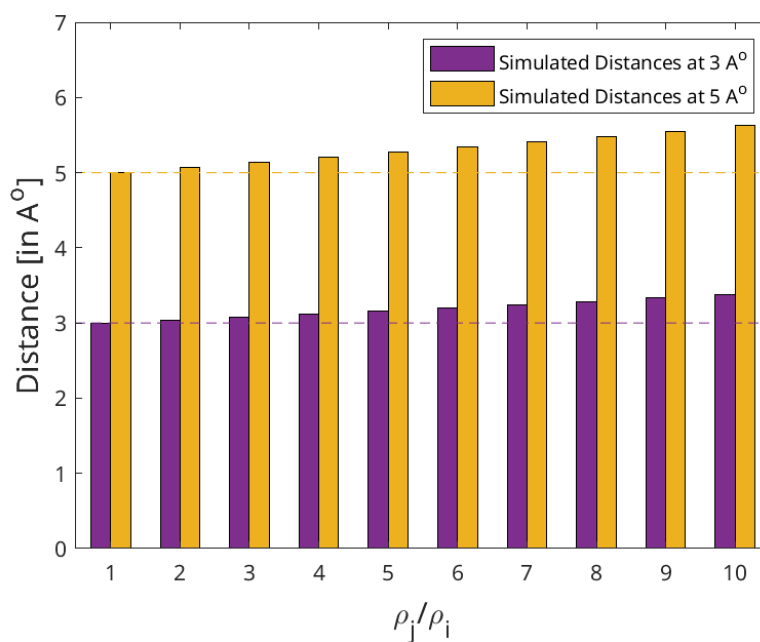
Figure A2: The effect of the relative auto-relaxation rates of the protein and the ligand on the distances extracted via the diagonal-normalised approach. The dotted lines represent the artificial distances 3Å and 5Å in purple and yellow respectively. The corresponding bars denote the distances back-calculated using the diagonal-normalised approach from the artificial distances depending on the the relative auto-relaxation rates, ρ_i and ρ_j. Each set of distances (bars) are derived through varying assumptions of the values of ρ_i and ρ_j with respect to each other ranging from $\frac{\rho_j}{\rho_i} = [1 \text{ to } 10]$.
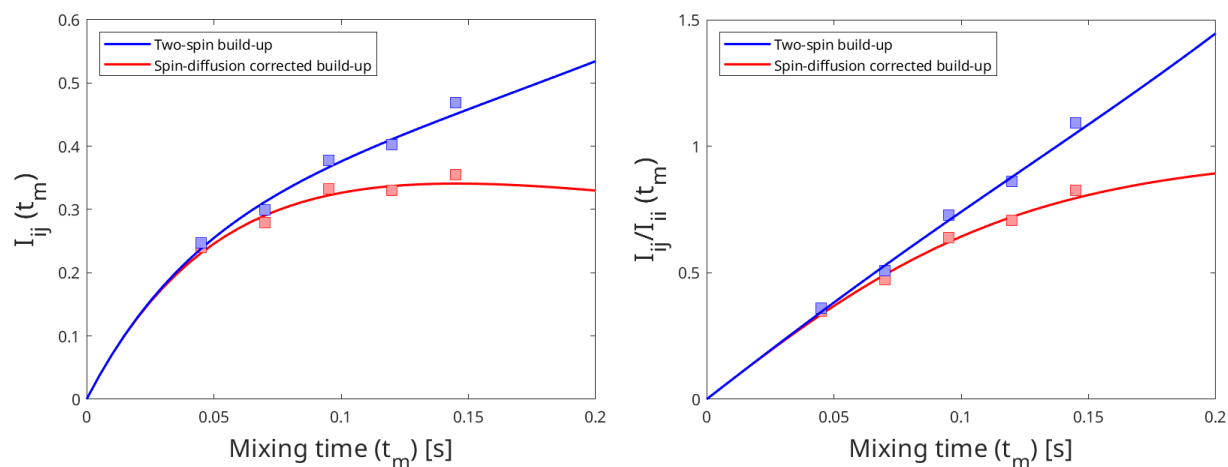
Figure A3: Effect of spin diffusion on the intensity build-up curves produced from eNORA-based approach (left) and diagonal-normalised approach (right). The build-up curves were fitted using artificially simulated peak intensities in a model system, Third Immunoglobulin Binding Domain of Protein G (GB3), which has been extensively studied using eNOE spectroscopy (Vögeli et al., 2012); (Vögeli et al., 2013). The blue curve represents the intensity build-up in an isolated two-spin system with an inter-proton distance of 3.83$\mathring{A}$ and the red curve represents the same two spins experiencing spin-diffusion due to presence of other spins in the system. The comparison between the plots highlight that it is easier to detect the influence of spin-diffusion with the diagonal-normalised approach (right), as it induces deviation from the expected linear fit.
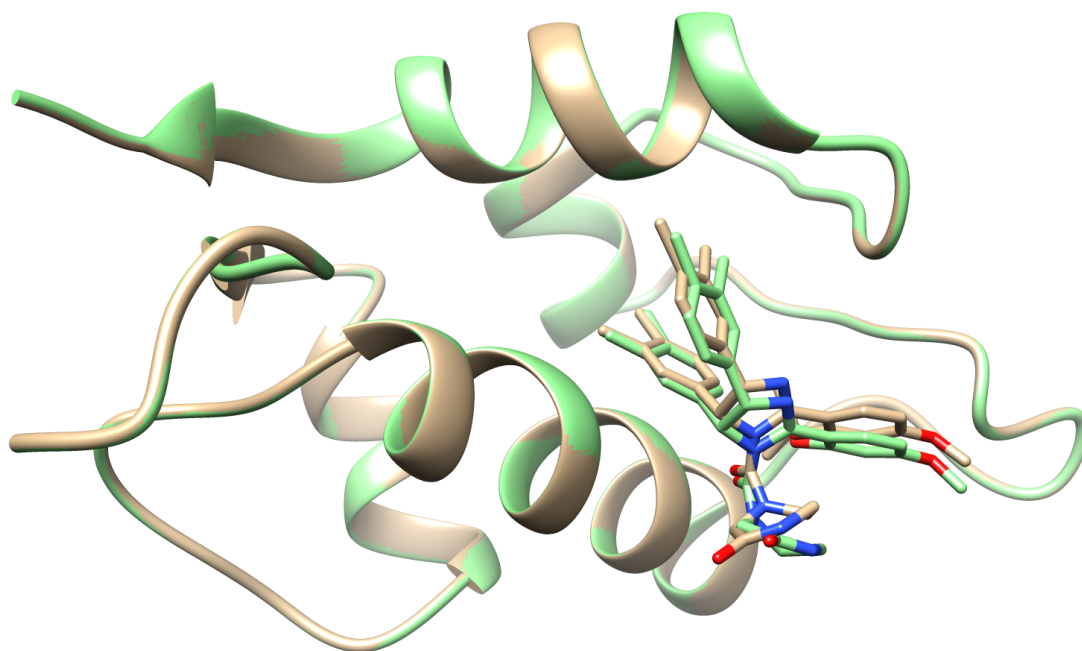
Figure A4: Ribbon representation of the protein, HDM2, with the stick representation of caylin-1 present in the binding pocket. Coloured in brown is the surface of the structure determined by traditional NMR^2 (7QDQ) by Mertens et al. (Mertens et al., 2022). Coloured in green is the structure determined by NMR^2 calculations using the the diagonal-normalised approach with a precision of 10%. The nitrogen and oxygen atoms on the ligand are coloured blue and red respectively.